Experimental Verification of the Chemical Sensitivity of Two-Site Double Core-Hole States Formed by an X-Ray Free-Electron Laser

P. Salén,[1,*] P. van der Meulen,[1] H. T. Schmidt,[1] R. D. Thomas,[1] M. Larsson,[1] R. Feifel,[2] M. N. Piancastelli,[2,†]
L. Fang,[3] B. Murphy,[3] T. Osipov,[3] N. Berrah,[3] E. Kukk,[4] K. Ueda,[5] J. D. Bozek,[6] C. Bostedt,[6] S. Wada,[6,7]
R. Richter,[8] V. Feyer,[8] and K. C. Prince[8,9]

[1]*Physics Department, Stockholm University, 106 91 Stockholm, Sweden*
[2]*Department of Physics and Astronomy, Uppsala University, 751 20 Uppsala, Sweden*
[3]*Physics Department, Western Michigan University, Kalamazoo, Michigan 49008, USA*
[4]*Department of Physics and Astronomy, University of Turku, 20014 Turku, Finland*
[5]*IMRAM, Tohoku University, Sendai 980-8577, Japan*
[6]*SLAC, LCLS, Menlo Park, California 94025, USA*
[7]*Department of Physical Science, Hiroshima University, Higashi-Hiroshima 739-8526, Japan*
[8]*Sincrotrone Trieste, 34149 Basovizza, Trieste, Italy*
[9]*IOM-CNR, 34149 Basovizza, Trieste, Italy*
(Received 14 October 2011; published 13 April 2012; corrected 1 May 2012)

We have performed x-ray two-photon photoelectron spectroscopy using the Linac Coherent Light Source x-ray free-electron laser in order to study double core-hole (DCH) states of CO_2, N_2O, and N_2. The experiment verifies the theory behind the chemical sensitivity of two-site DCH states by comparing a set of small molecules with respect to the energy shift of the two-site DCH state and by extracting the relevant parameters from this shift.

The Linac Coherent Light Source (LCLS) x-ray free-electron laser, at the SLAC National Accelerator Laboratory, produces ultrashort laser pulses with extremely high peak intensities in both the soft and hard x-ray domain [1,2]. These characteristics enable the exploration of hitherto virtually unmapped scientific territories, such as the nonlinear interaction between matter and x-ray photons, and allows for a natural continuation of the already well established field of optical nonlinear laser spectroscopy [3]. An intriguing example of such an x-ray-induced multiphoton process is the production of double core-hole (DCH) states via the sequential absorption of two soft-x-ray photons on a time scale on the order of the molecular Auger lifetime (~ 4–8 fs) [4]. The formation of molecular two-site (TS) DCH states, in particular, shows great promise as a powerful tool for chemical analysis [5,6], and recently has attracted considerable attention [7–10]. The unique properties of the LCLS permit the search for these double core vacancies located at different atomic sites using x-ray two-photon photoelectron spectroscopy [11–14].

A compelling motivation for the study of TSDCH states is their ability to probe the local chemical environment more sensitively than either single core-hole (SCH) [15] or single-site (SS) DCH [16–18] states as predicted by Cederbaum *et al.* in their seminal paper from 25 years ago [5]. Their results were confirmed recently by Tashiro *et al.* [6] who calculated the single ionization potentials (IP) and double core-hole ionization potentials (DIP) for a series of small molecules. The increased sensitivity originates from the fact that the DIP of TSDCH states is

directly coupled to induced changes in the valence charge distribution at the two different atomic sites [6]. Here we set out to verify these theoretical predictions by measuring the DIPs of the TSDCH states for a set of small molecules, viz. N_2, N_2O, CO_2, and CO [8].

The experiments reported here [19] were performed using the atomic, molecular, and optical instrument [20,21] of the LCLS. The free-electron laser generated light pulses with a FWHM (full width at half maximum) duration of ~10 fs, a photon energy of between 517 and 705($\pm$15) eV, and a pulse energy of approximately 30 μJ on the target. A tightly focused laser beam provided the high intensity in the interaction region (3×10^{16} W/cm^2) that enabled sequential ionization of the molecules. Data taken with an unfocused beam (1×10^{14} W/cm^2) were subtracted from data taken with the focused beam in order to extract the nonlinear contributions to the photoelectron signal, and more clearly observe the DCH states.

In the difference spectra, a number of features can be discerned that are unambiguously related to the sequential absorption of two soft x-ray photons. First, at kinetic energies that are about 50–100 eV lower than the ordinary $1s^{-1}$ photoline (depending on the atom involved) a peak is observed that can be confidently assigned to the SSDCH state [6]. The TSDCH states are located much closer to the main photoline, typically shifted to lower energy by about 10–20 eV [6]. If the pulse duration exceeds the Auger lifetime, Auger decay can take place before the absorption of a second photon. This gives rise to the so-called photoemission-auger-photoemission (PAP)

peaks in the photoelectron spectra, whose location can be calculated from the energies of the relevant doubly and triply ionized states of the molecule [10,18,22–24]. Generally, PAP peaks appear at kinetic energies of about 20–40 eV lower than the main photoline.

The relative intensities of the SSDCH, TSDCH, and PAP peaks, as well as that of the main photoline, can be simulated on the basis of a straightforward kinetic model which has been shown to produce reliable results [25]. For our experimental conditions and for the molecules studied here, the various SSDCH and TSDCH peaks for a particular molecule are expected to have very similar integrated intensities, typically within a factor of 2 [19]. This means that the presence of the usually easily identifiable SSDCH peak implies the existence of a roughly equally intense TSDCH peak. This is of great help in analyzing the spectra because the latter generally lies in a more congested region of the photoelectron spectrum. The relative intensity of the PAP peaks is calculated to be comparable to that of the DCH lines [19].

The most prominent DCH structures were observed in N_2 and we begin the discussion with N_2 and N_2O, before we continue with our observations of DCHs in CO_2 and CO [8].

Figure 1(a) shows the photoelectron spectra of N_2 at kinetic energies below the N SCH peak at 186 eV, where the DCH features are expected to lie. The photon energy was 596 eV and the electron time-of-flight (eTOF) spectrometer was oriented at the magic angle (54.7° with respect to the polarization of the laser beam). The blue and green spectra correspond to data taken with the focused and unfocused beams, respectively, and are normalized to the N SCH peak. The magenta spectrum plots the difference between these data to highlight nonlinear

contributions to the signal, i.e., the DCHs. The experimentally determined positions of the nonlinear peaks are indicated in Fig. 1(a) by the black vertical lines (the estimated error is represented by the horizontal line) together with the theoretically predicted positions [6] (yellow vertical lines). The energy resolution is ~4.6 eV given by the FWHM of the N SCH peak.

Data obtained with the unfocused beam are free from nonlinear contributions and comparable to data taken using synchrotron light [19], consisting of the N SCH peak and its shakeup and shakeoff satellites. The largest satellite intensity is expected at kinetic energies of about 155–175 eV [26,27] and such features are observed in both the focused and unfocused spectra [Fig. 1(a)]. At lower electron kinetic energies one expects to find shakeoff and smaller satellites.

The difference spectrum in Fig. 1(a) clearly reveals three distinct features located at kinetic energies of ~102, ~155, and ~169 eV. These correspond to the SSDCH, PAP, and TSDCH states, respectively. A continuous background also appears in this difference spectrum, as well as in the spectra of the other measured molecules. Its origin is not entirely clear but the background may partly arise from atomic ions produced by rapid fragmentation [8], satellites, including shakeoff, to the PAP and DCH peaks, or may be related to secondary electrons that are not completely eliminated in the subtraction procedure due to the different source volumes in the focused and unfocused measurements.

Figure 1(b) shows the corresponding photoelectron spectra for N_2O. The photon energy in these measurements was 517 eV, i.e., below the ionization limit of O $1s$ electrons in order to generate signals solely from N related DCHs. This facilitates easier comparison between the
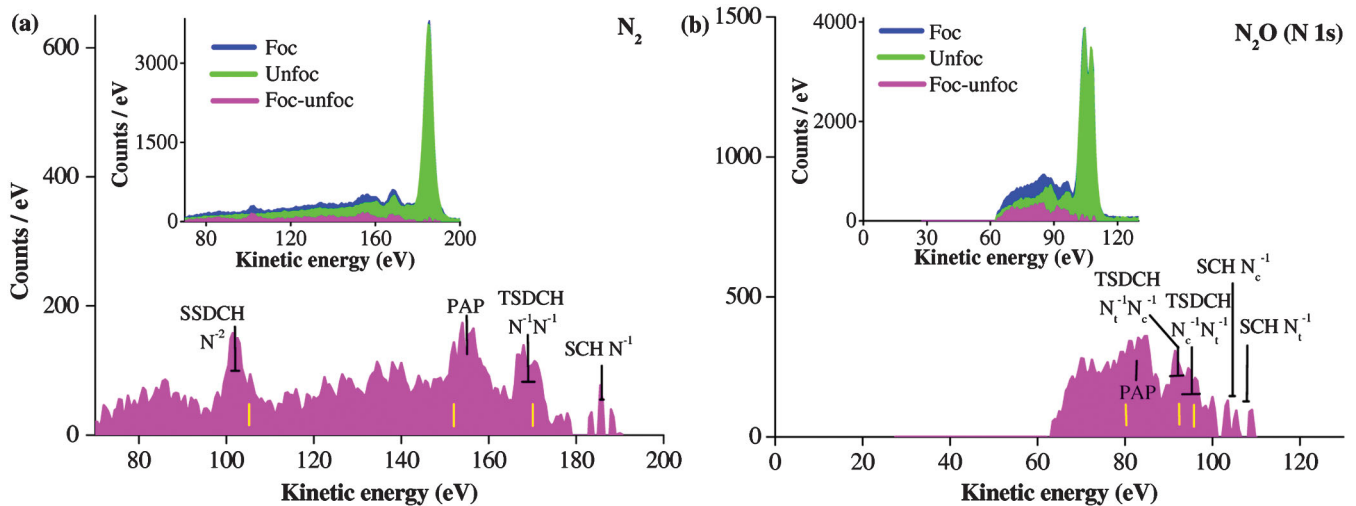

FIG. 1 (color).   Photoelectron spectra of N_2 (a) and N_2O (b) with a photon energy of 596 eV and 517 eV, respectively. Blue curve: focused x rays; green curve unfocused; spectra are normalized at the SCH peak. Magenta curve: difference spectra. Black vertical lines: experimental energies of the SCH, DCH, and PAP features; horizontal lines: estimated errors; yellow vertical lines: theoretical energies [6].

$N^{-1}N^{-1}$ TSDCH in N_2 and N_2O. (For the photoelectron spectra of N_2O obtained using a photon energy of 597 eV, i.e., above the O $1s$ ionization limit, see Supplemental material [19]). The kinetic-energy region of interest is smaller for N_2O than N_2, due to the reduced photon energy, but for ease of comparison the same kinetic-energy scale as in Fig. 1(a) is used. The reduced photon energy also results in an increased energy resolution, ~4 eV, compared with that observed for N_2.

The asymmetry of N_2O, with one central (N_c) and one terminal (N_t) N atom, manifests itself in a splitting of the N SCH peak of about 4.0 eV. The difference spectrum shows similar structures to those observed in N_2: a TSDCH peak followed by a PAP peak. The position of the experimentally observed TSDCH peak is in good agreement with the calculated value [6]. This peak consists of contributions from the $N_c^{-1}N_t^{-1}$ (N_c followed by N_t core-ionization) and $N_t^{-1}N_c^{-1}$ (N_t followed by N_c core-ionization) state, which seem to be just resolved. The marked experimental positions are also reasonable given the expected separation of 4 eV between the two peaks.

Table I lists the single (IP) and double ionization potentials (DIP) for the SCH and DCH states, respectively. The DIPs are derived from the energy shifts of the SSDCH (ΔE_1) and TSDCH (ΔE_2) states, where $\Delta E_1 = \mathrm{DIP}(S^{-2})\text{-}2\mathrm{IP}(S^{-1})$ and $\Delta E_2 = \mathrm{DIP}(S_i^{-1}, S_j^{-1})\text{-}\mathrm{IP}(S_i^{-1})\text{-}\mathrm{IP}(S_j^{-1})$, which are directly determined from the spectra as the shift with respect to the SCH line. These

values are also listed together with the DIPs and they all agree reasonably well with their corresponding theoretical values. The chemical sensitivity of the TSDCH states is reflected in the value of ΔE_2, and we determine that ΔE_2 is lower by 3.7 ± 2.7 eV for $N_c^{-1}N_t^{-1}$ in N_2O compared with the $N^{-1}N^{-1}$ state in N_2, in tolerable agreement with the calculated difference (2.2 eV) [6]. This lowering is due to the influence of the extra O atom.

The predicted high sensitivity of the TSDCHs to the chemical environment is related to the flow of electron density in the creation of the TSDCH states [6]. This change of electron density may be quantified by the generalized interatomic relaxation energy (IRC) [6], which is related to ΔE_2 according to $\Delta E_2 = 1/r\text{-IRC}$, where r is the distance between the two core holes. The decrease in ΔE_2 of N_2O and CO_2 with respect to N_2 and CO due to the change in bond length $(1/r)$ related to an extra O atom is approximately 0.4 eV [31]. Values of IRC are given in Table I. Theory predicts a modest difference between the IRC of the $N^{-1}N^{-1}$ TSDCH in N_2 and N_2O. This is manifested experimentally by the relatively small difference of ΔE_2 (3.7 eV) between the two states, which is only slightly larger than the difference in the IPs of N in N_2 and N_2O, respectively. The effect is, however, more pronounced in the case of CO and CO_2, as we will show later.

For diatomic molecules, creation of the core hole decreases the electron density on the other atom and thus the relaxation is suppressed for the core-hole creation of

TABLE I. Experimental and theoretical ionization potentials as well as ΔE_1, ΔE_2, and the IRC [6] (see text), for states of N_2, N_2O, CO_2, and CO. IP(S^{-1}): SCH ionization potential, DIP(S^{-2}): SSDCH double ionization potential, DIP(S_i^{-1}, S_j^{-1}): TSDCH double ionization potential. Experimental DIPs are calculated as the sum of the experimental IP(S^{-1}), calibrated to known values, and the relevant IP of the ion, determined in our experiments. The experimental value of the IP for CO (O $1s$) = 542.5 eV was taken from Ref. [28]. Errors are calculated as the root mean square of the estimated errors for the positions of the spectral peaks.

Molecule	IP(S^{-1}) (eV)	DIP(S^{-2}) (eV)	DIP(S_i^{-1}, S_j^{-1}) (eV)	$\Delta E_1(S^{-2})$ (eV)	$\Delta E_2(S_i^{-1}, S_j^{-1})$ (eV)	IRC (eV)
N_2	(N^{-1})	(N^{-2})	($N^{-1}N^{-1}$)	(N^{-2})	($N^{-1}N^{-1}$)	($N^{-1}N^{-1}$)
Exp.	409.9 ± 0.3 [29]	903.2 ± 1.1	836.2 ± 1.6	83.4 ± 1.1	16.4 ± 1.6	-3.29 ± 1.6
Theory [6]	411.0	901.2	836.4	79.2	14.3	-0.65
N_2O (N_t)	(N_t^{-1})	(N_t^{-2})	($N_c^{-1}N_t^{-1}$)	(N_t^{-2})	($N_c^{-1}N_t^{-1}$)	($N_c^{-1}N_t^{-1}$)
Exp.	409.0 ± 0.5		834.2 ± 2.1		12.7 ± 2.1	0.09 ± 2.1
Theory [6]	408.6	893.9	833.2	76.7	12.1	1.11
N_2O (N_c)	(N_c^{-1})	(N_c^{-2})	($N_t^{-1}N_c^{-1}$)	(N_c^{-2})	($N_t^{-1}N_c^{-1}$)	($N_t^{-1}N_c^{-1}$)
Exp.	412.5 ± 0.5 [29]		834.2 ± 1.6		12.7 ± 1.6	0.09 ± 1.6
Theory [6]	412.5	902.3	833.2	77.3	12.1	1.11
CO_2 (O $1s$)	(O^{-1})	(O^{-2})		(O^{-2})	($O^{-1}O^{-1} + C^{-1}O^{-1}$)	
Exp.	540.6 ± 0.5 [30]	1173.2 ± 1.6		92.0 ± 1.5	12.8 ± 1.6	
Theory [6]	542.9	1171.9		86.2	9.1	
CO_2 (C $1s$)	(C^{-1})	(C^{-2})	($O^{-1}C^{-1}$)	(C^{-2})	($O^{-1}C^{-1}$)	($O^{-1}C^{-1}$)
Exp.	296.8 ± 0.5 [30]		848.6 ± 1.6		11.2 ± 1.6	1.21 ± 1.6
Theory [6]	297.6	664.6	851.2	69.3	10.6	1.79
CO (C $1s$)	(C^{-1})	(C^{-2})	($O^{-1}C^{-1}$)	(C^{-2})	($O^{-1}C^{-1}$)	($O^{-1}C^{-1}$)
Exp. [8]	296.5 ± 0.5	667.9 ± 3.6	855.3 ± 1.2	74.9 ± 4.0	16.3 ± 1.2	-3.53 ± 1.2
Theory [6]	296.4	664.4	855.2	71.7	15.9	-2.8

the second atom, resulting in a negative IRC. For triatomic molecules, in which one of the core holes is located at the center atom, the extra not core ionized atom plays the role of an electron donor to the other two atoms with core holes and enhances the relaxation of the double core hole at the other two sites, resulting in a positive IRC. We find that the relaxation is suppressed (IRC < 0) for N_2 and enhanced (IRC > 0) for N_2O, as predicted [6].

Comparison between data obtained for CO and CO_2 allows the influence of the extra O atom in CO_2 on the $O^{-1}C^{-1}$ TSDCH state to be investigated. The photoelectron spectra of CO, in which the $O^{-1}C^{-1}$ TSDCH was positively identified, was recently reported by Berrah *et al.* [8], and we here present the data obtained for CO_2.

The measurements on CO_2 were recorded with an *e*TOF oriented parallel to the polarization of the laser. As in Fig. 1, Fig. 2(a) shows the photoelectron spectra of CO_2 for kinetic energies below the O SCH peak at 165 eV and were obtained using a photon energy of 705 eV. The assignments of the peaks are marked in the figure. For the peak at ~152 eV, theory predicts contributions from two close lying TSDCH states separated by ~2 eV [6]. One arises when a 1s electron is ejected from each O atom ($O^{-1}O^{-1}$) and the other when the first electron originates from the C atom and the second from one of the O atoms ($C^{-1}O^{-1}$). However, the energy resolution here is ~5 eV, and we do not resolve these contributions.

The spectra shown in Fig. 2(b) were taken in the same measurement as Fig. 2(a) but now we highlight the kinetic-energy region near the C SCH peak. Here one expects to find only one TSDCH peak, arising from the $O^{-1}C^{-1}$ state. This peak appears at the calculated position in the difference spectrum [see Fig. 2(b)]. The PAP peak is also

observed, but the carbon $(1s)^{-2}$ SSDCH peak cannot be positively identified. This is in full agreement with our simulations which indicate a much reduced intensity for this particular feature [19]. Note that in general the DCH photoelectron spectrum of a homonuclear diatomic molecule, e.g., N_2, contains a smaller number of peaks compared to that of a similar heteronuclear diatomic molecule, such as CO. The concentration of nonlinear intensity into fewer peaks will often make the DCH features stand out more clearly in the former case.

The DCH features for N_2O and CO_2 are less pronounced than in the case of N_2 mainly due to the operating conditions of the LCLS at the time these measurements were made. However, our assignments are supported strongly not only by the calculated peak positions [6,8,18,22–24] but also by our simulations of the expected relative intensities of the SSDCH, PAP, TSDCH, and SCH peaks [19]. In addition, the experimental results for N_2 clearly establish the principle, and the pattern with SSDCH, PAP, and TSDCH peaks is repeated for all molecules.

Table I lists the IPs and DIPs for the SCH and DCH states together with ΔE_1 and ΔE_2 for CO_2 and CO. Table I also lists the results from both the O 1s and C 1s peaks of CO_2, although the observed TSDCH peak adjacent to the O 1s line cannot be resolved into its two components, and is not used for comparison with CO. The TSDCH peak close to the C 1s line consists of only one contribution, that from $O^{-1}C^{-1}$, and is suitable for extracting ΔE_2. Comparing ΔE_2 for the $O^{-1}C^{-1}$ TSDCH state of CO and CO_2 allows us to evaluate experimentally the environmental effect of the extra O atom in CO_2. Here, ΔE_2 for the $O^{-1}C^{-1}$ TSDCH state of CO_2 is 5.1 ± 2.3 eV lower than that of CO, in good agreement with the predicted value of 5.3 eV [6]. It is noted that the IP difference between C^{-1} SCH
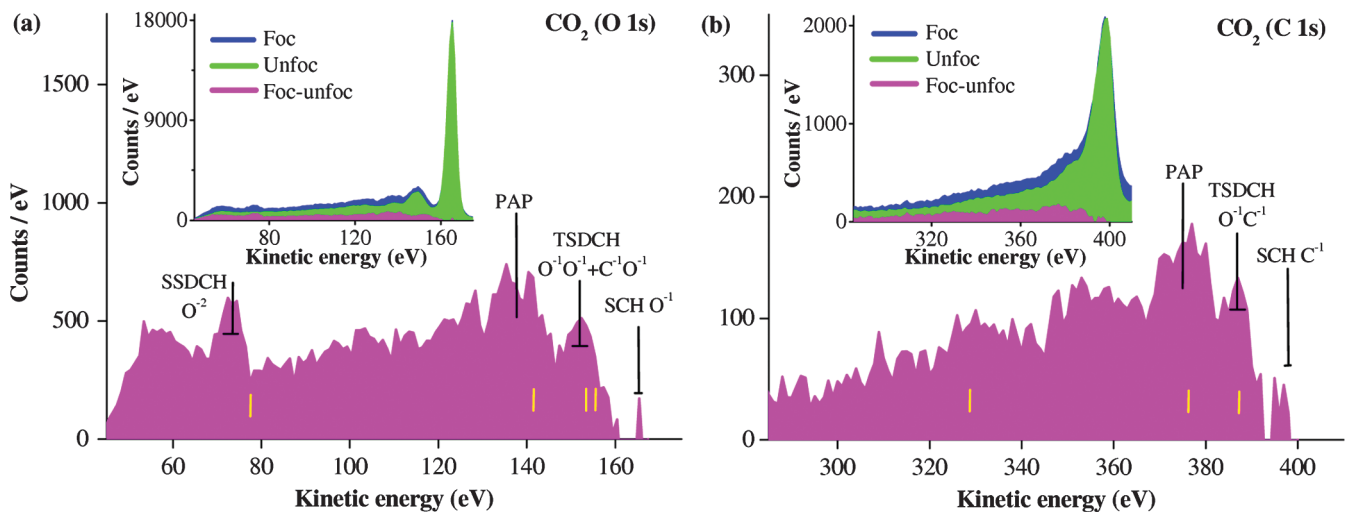

FIG. 2 (color).   Photoelectron spectra of CO_2 near the O SCH line (a) and C SCH line (b), photon energy 705 eV. Blue curve: focused x rays; green curve: unfocused x rays; spectra are normalized at the SCH peak. Magenta curve: difference spectrum. Black vertical lines: experimental energies of the SCH, DCH, and PAP features; horizontal lines: estimated errors; yellow vertical lines: theoretical energies [6].

states in CO and CO_2 is only 0.3 eV, while the DIP difference between the $O^{-1}C^{-1}$ TSDCH states is 6.7 eV. The higher sensitivity of TSDCH states, by an order of magnitude, to the chemical environment is evident.

If we focus on the IRC values given in Table I we find that the large difference in IRC between the $O^{-1}C^{-1}$ state of CO and CO_2, compared with the case of N_2 and N_2O, which results in the large shift of ΔE_2 in the former case, fits nicely with theory [6]. In addition we find also for these two molecules that the relaxation is suppressed (IRC $<$ 0) for the diatomic CO and enhanced (IRC $>$ 0) for the triatomic CO_2, as predicted [6].

In conclusion, we have presented evidence for the formation of TSDCH states in the molecules N_2, N_2O, and CO_2 by employing photoelectron spectroscopy using a free-electron laser x-ray light source. Our experimental results for the DIP, ΔE_2, and IRC reproduce the trends predicted by the theory for TSDCH states [6], and thus support its main implication that the TSDCH states are extra sensitive to the chemical environment. In particular, the IRC, a characteristic parameter of the TSDCH states, was found to behave according to theory. The sensitivity of the TSDCH state to the chemical environment was exemplified by the large spectral shift of the $O^{-1}C^{-1}$ TSDCH state in CO_2 compared with CO, which is induced by the extra O atom.

*peter.salen@fysik.su.se

†Present address: Université Pierre et Marie Curie, Laboratoire de Chimie Physique-Matière et Rayonnement, UMR 7614, 75231 Paris Cedex 05, France

[1] P. Emma *et al.*, Nature Photon. **4**, 641 (2010).
[2] I. A. Vartanyants *et al.*, Phys. Rev. Lett. **107**, 144801 (2011).
[3] S. Mukamel, *Principles of Nonlinear Optical Spectroscopy* (Oxford University Press, New York, 1995).
[4] K. C. Prince, M. Vondráček, J. Karvonen, M. Coreno, R. Camilloni, L. Avaldi, and M. de Simone, J. Electron Spectrosc. Relat. Phenom. **101-103,** 141 (1999).
[5] L. S. Cederbaum, F. Tarantelli, A. Sgamellotti, and J. Schirmer, J. Chem. Phys. **85,** 6513 (1986).
[6] M. Tashiro, M. Ehara, H. Fukuzawa, K. Ueda, C. Buth, N. V. Kryshevoi, and L. S. Cederbaum, J. Chem. Phys. **132,** 184302 (2010).
[7] L. Fang *et al.*, Phys. Rev. Lett. **105,** 083005 (2010).
[8] N. Berrah *et al.*, Proc. Natl. Acad. Sci. U.S.A. **108,** 16912 (2011).
[9] M. Gudmundsson, D. Fischer, D. Misra, A. Källberg, A. Simonsson, K. Støchkel, H. Cederquist, and H. T. Schmidt, J. Phys. B **44,** 175201 (2011).
[10] P. Lablanquie *et al.*, Phys. Rev. Lett. **107,** 193004 (2011).
[11] R. Santra, N. V. Kryzhevoi, and L. S. Cederbaum, Phys. Rev. Lett. **103,** 013002 (2009).
[12] N. V. Kryzhevoi, R. Santra, and L. S. Cederbaum, J. Chem. Phys. **135,** 084302 (2011).
[13] M. Hoener *et al.*, Phys. Rev. Lett. **104,** 253002 (2010).
[14] J. P. Cryan *et al.*, Phys. Rev. Lett. **105,** 083004 (2010).
[15] K. Siegbahn, Rev. Mod. Phys. **54,** 709 (1982).
[16] J. H. D. Eland, M. Tashiro, P. Linusson, M. Ehara, K. Ueda, and R. Feifel, Phys. Rev. Lett. **105,** 213005 (2010).
[17] P. Linusson, O. Takahashi, K. Ueda, J. H. D. Eland, and R. Feifel, Phys. Rev. A **83,** 022506 (2011).
[18] P. Lablanquie *et al.*, Phys. Rev. Lett. **106,** 063003 (2011).
[19] See Supplemental Material at http://link.aps.org/supplemental/10.1103/PhysRevLett.108.153003 for full details of experiment and supporting results.
[20] J. D. Bozek, Eur. Phys. J. Special Topics **169,** 129 (2009).
[21] O. Hemmers, S. Whitfield, P. Glans, H. Wang, D. W. Lindle, R. Wehlitz, and I. A. Sellin, Rev. Sci. Instrum. **69,** 3809 (1998).
[22] J. H. D. Eland, Chem. Phys. **294,** 171 (2003).
[23] A. E. Slattery, T. A. Field, M. Ahmad, R. I. Hall, J. Lambourne, F. Penent, P. Lablanquie, and J. H. D Eland, J. Chem. Phys. **122,** 084317 (2005).
[24] M. Tashiro, K. Ueda, and M. Ehara (to be published).
[25] N. Rohringer and R. Santra, Phys. Rev. A **76,** 033416 (2007).
[26] S. Svensson, A. Naves de Brito, M. P. Keane, N. Correia, L. Karlsson, C.-M. Liegener, and H. Ågren, J. Phys. B **25,** 135 (1992).
[27] B. Kempgens, A. Kivimäki, M. Neeb, H. M. Köppe, A. M. Bradshaw, and J. Feldhaus, J. Phys. B **29,** 5389 (1996).
[28] A. A. Bakke, H. Chen, and W. L. Jolly, J. Electron Spectrosc. Relat. Phenom. **20,** 333 (1980).
[29] M. Alagia *et al.*, Phys. Rev. A **71,** 012506 (2005).
[30] T. Hatamoto *et al.*, J. Electron Spectrosc. Relat. Phenom. **155,** 54 (2007).
[31] Bondlengths can be found at: http://cccbdb.nist.gov/